

Kinetic modeling of scrape-off layer plasmas

K. Kupfer,^{a)} R. W. Harvey,^{b)} O. Sauter,^{c)} M. J. Schaffer, and G. M. Staebler
General Atomics, San Diego, California 92186-9784

(Received 5 February 1996; accepted 11 July 1996)

Electron transport along open field lines in the diverted scrape-off layer of a tokamak is studied numerically via a kinetic Fokker–Planck approach. The method allows calculation of the distribution function in a situation where large parallel temperature gradients are maintained by collisional relaxation and, at the same time, superthermal electrons stream freely from the midplane of the plasma to the target/sheath boundary. The method also allows calculation of the self-consistent electrostatic field associated with parallel gradients in the distribution function, as well as the potential drop across the target/sheath boundary, where the latter is calculated to enforce appropriate boundary conditions at the target, although the sheath itself is not resolved. The kinetic results are compared to classical fluid results for the case of a simple (nonradiative) divertor. The kinetic solutions exhibit an enhanced superthermal electron population in the vicinity of the target, which results in a larger sheath energy transmission factor, a lower bulk electron temperature, and a smaller sheath potential drop. The sheath potential largely determines the energy with which ions impact the target, thereby affecting the rate of target erosion. Ionization rates and radiation rates from impurities in the vicinity of the target also depend strongly on the local electron temperature and can be sensitive to superthermal tails. © 1996 American Institute of Physics.
[S1070-664X(96)03710-X]

I. INTRODUCTION

Successful operation of a tokamak fusion device requires maintaining a clean hot plasma core, while minimizing erosion of the divertor target. This depends critically on plasma parameters in the scrape-off layer (SOL), where a large heat flux is carried along open magnetic field lines to the divertor. A substantial portion of this heat flux is carried by electrons, making electron heat conduction an important divertor physics issue.

It is well known that parallel electron heat transport in a magnetized plasma is sensitive to long mean free path effects that are outside the scope of conventional fluid theory. For classical electron thermal conductivity to be valid, the electron mean free path (MFP) must be suitably small compared to the temperature gradient scale length.¹ In the long MFP regime, early numerical work showed that the conductive heat flux remains limited to a fraction of the free-streaming flux $n_e T_e v_e$.² Based on heuristic arguments and numerical solutions, researchers attempted to construct a nonlocal model linking the heat flux to the temperature profile.³ This line of research was later extended by more detailed analysis of the Fokker–Planck equation.^{4–8} In all of this work, the breakdown of conventional fluid theory occurs even while the MFP of *thermal* electrons is short compared to the temperature gradient scale length. This is because most of the heat flux is carried by *energetic* electrons whose velocities are in the range $3v_e$ [where $v_e = (T_e/m_e)^{1/2}$]. These particles

have a MFP roughly 80 times that of thermal particles, i.e., the MFP scales like $(v/v_e)^4$, thereby allowing superthermal electrons to free stream over a substantial portion of the temperature gradient. For typical parameters in the SOL, this results in a competition between collisions and free streaming. Bulk collisions are responsible for maintaining the temperature gradient, while free streaming replenishes the target region with energetic electrons from the midplane. The physics of the target/sheath region determines the boundary value of the electron temperature for a given heat flux and particle flux. This boundary physics is sensitive to the influx of hot electrons from the midplane of the plasma.

Research in this area has generally relied on test-particle Monte Carlo simulations.^{9,10} The drawback of this method is that the self-consistent temperature profile remains undetermined. While the test-particle method seeks to characterize the relation between the heat flux and the temperature profile, it does so for an artificial state of the system, without satisfying the appropriate boundary conditions. As an alternative to this method, self-consistent solutions have been obtained with a multispecies particle-in-cell code,^{11,12} but code runs are expensive and have typically covered only a few centimeters of field line in front of the target, whereas the region of interest typically extends for tens of meters. The goal of this paper is to present a set of self-consistent numerical solutions of the electron Fokker–Planck equation, extending along the SOL from the midplane, into the divertor, and to the target/sheath boundary. To do this, we have developed the Fokker–Planck edge transport code (FPET), a fully kinetic parallel transport code which solves for $f(v_\perp, v_\parallel, z)$, the gyroaveraged distribution function along a magnetic field line. Although the numerical techniques employed here are a straightforward extension of earlier work,¹³ we describe a new procedure for implementing quasineutral-

^{a)}Oak Ridge Institute for Science and Education Postdoctoral Fellow at General Atomics. Present address: Southwestern Medical Center at Dallas, McDermott Center for Human Growth and Development, 5323 Harry Hines Blvd., Dallas, Texas 75235-8591.

^{b)}Present address: CompX, 12839 Via Grimaldi, Del Mar, California 92014.

^{c)}Permanent address: Centre de Recherches en Physique des Plasmas/EPFL, Lausanne, Switzerland.

ity, thereby allowing calculation of the self-consistent electric field.

Classical fluid theory for a simple (nonradiative) divertor is reviewed in Sec. II. The kinetic approach is outlined in Sec. III. Details of the numerical method are discussed in Sec. IV. The results, comparing kinetic and fluid solutions, are presented in Sec. V. Conclusions are given in Sec. VI.

II. CLASSICAL FLUID APPROACH

Here we discuss conventional fluid theory for parallel transport in a simple divertor. In this approach, one assumes the classical relation for parallel heat conduction together with an appropriate target/sheath boundary condition. The sheath region is treated as a boundary layer wherein the distribution function is assumed to be Maxwellian. Results obtained in this section will be referred to as ‘‘classical’’ to distinguish them from the kinetic results obtained in subsequent sections. If q_e denotes the electron heat flux parallel to the magnetic field and κ denotes the plasma thermal conductivity, then the classical relation for T_e is

$$q_e = -\kappa \nabla_{\parallel} T_e. \quad (1)$$

Braginskii gives $\kappa = 3.16 (n_e \tau_e T_e / m_e)$ where $\tau_e = 3(m_e)^{1/2} T_e^{3/2} / [4(2\pi)^{1/2} \ln \Lambda e^4 n_e]$ is the electron collision time¹⁴ and Z_i is assumed to be unity. In the absence of sources and sinks and neglecting any convective flux, the steady-state solution of the heat equation requires constant q_e . Taking q_e constant and neglecting variations in $\ln \Lambda$, Eq. (1) is easily integrated to obtain

$$T_e = T_{e0} (1 - z/D)^{2/7}, \quad (2)$$

where z is the distance along the magnetic field line measured upstream (negative) from the target at $z=0$. Here $D = \kappa_0 T_{e0} / (3.5 q_e)$, where T_{e0} and κ_0 are the electron temperature and thermal conductivity evaluated at the target/sheath boundary. The classical solution thus reduces to a set of profiles whose steepness is controlled by a single parameter D .

Equation (1) can be rewritten in the following form:

$$q_e / (n_e T_e v_e) = 3.16 \lambda_e / L_T, \quad (3)$$

where $L_T \equiv T_e |dT_e/dz|^{-1}$ is the gradient length of the temperature profile, $\lambda_e = \tau_e v_e$ is the thermal MFP, and $v_e = (T_e/m_e)^{1/2}$ is the thermal velocity. In Ref. 8, the breakdown of Eq. (1) is shown to occur for $\lambda_e \geq 5.3 \times 10^{-2} L_T$, where the numerical factor of 5.3 accounts for differences in the definition of MFP. Substituting this constraint into Eq. (3) gives $q_e / (n_e T_e v_e) \leq 0.17$ as the valid regime for classical fluid theory. In Ref. 9, Monte Carlo solutions of the Fokker-Planck equation show the breakdown of Eq. (3) and the presence of a flux limit, whereby $q_e / (n_e T_e v_e) \leq C_{\text{fl}}$, with C_{fl} a numerical coefficient typically in the range of 0.1–0.2.

At this stage arbitrary collisionality regimes are possible, since for any given temperature profile, the density can be decreased, thereby increasing the MFP until Eq. (3) is violated. In fact, however, proper treatment of the target/sheath boundary results in an additional constraint which limits the collisionality. Assuming that the target floats electrostatically, at steady state the electron and ion fluxes through the

sheath must be balanced, i.e., ambipolar. Furthermore, since the Bohm sheath criterion limits the ion flow velocity to be roughly Mach 1 at the entrance to the sheath (see the review in Ref. 15), one obtains a constraint on the electron flux. In particular, the electron flux through the sheath is

$$\Gamma_{e0} = M n_{e0} [(T_{e0} + T_{i0}) / m_i]^{1/2}, \quad (4)$$

where all plasma parameters are evaluated at the entrance to the sheath and M is a numerical coefficient of order unity. Throughout this paper, we ignore the length scale of the sheath (both the Debye sheath, as well as the ion gyrosheath) and instead we impose an appropriate boundary condition at $z=0$. Assuming a Maxwellian distribution at the target/sheath boundary gives the classical result

$$\phi = -\ln[\Gamma_{e0} (2\pi)^{1/2} / (n_{e0} v_{e0})], \quad (5)$$

where $\phi \equiv e \Delta \Phi_{\text{sh}} / T_{e0}$ is the normalized sheath potential and $v_{e0} = (T_{e0} / m_e)^{1/2}$. This follows from Eq. (4) by computing the integral

$$\Gamma_{e0} = \int 2\pi v_{\perp} dv_{\perp} \int_s^{\infty} dv_{\parallel} v_{\parallel} f_{e0}, \quad (6)$$

where f_{e0} is the electron distribution at the target/sheath boundary, $s = (2e \Delta \Phi_{\text{sh}} / m_e)^{1/2}$, and all electrons with $v_{\parallel} < s$ are reflected by the sheath potential. In the same fashion, we may also compute the electron heat flux through the sheath, i.e.,

$$q_{e0} = \int 2\pi v_{\perp} dv_{\perp} \int_s^{\infty} dv_{\parallel} v_{\parallel} \left(\frac{m_e v^2}{2} \right) f_{e0}. \quad (7)$$

It is convenient to define the sheath energy transmission factor

$$\delta \equiv q_{e0} / (\Gamma_{e0} T_{e0}). \quad (8)$$

Once again, assuming a Maxwellian distribution in Eq. (7), one obtains the classical result

$$\delta = \phi + 2. \quad (9)$$

In Eq. (4) we assume deuterium ions with $T_{i0} = T_{e0}$ and $M = 1$. Now substituting Eq. (4) into Eq. (5), the classical results are $\phi = 2.8$ and $\delta = 4.8$.

Further comment is needed on our implementation of the Bohm criterion [Eq. (4)] and our treatment of ions. The goal of this paper is to present a kinetic model for electrons and to compare the results of this model with classical fluid theory in a consistent fashion. Since the ions are not treated in detail, the precise value of the coefficient M in Eq. (4) cannot be determined, therefore, we take $M = 1$, a reasonable value. It should be noted, however, that the magnetic field in a divertor configuration generally intersects the target at an oblique angle, modifying the sheath physics and the value of M , as discussed, for example, in Refs. 16–19. Here we are effectively compressing both the Debye sheath and the ion gyrosheath into one boundary condition that requires specifying the electron flux to the target. Furthermore, we assume that there is a strong ionization source of electrons directly in front of the target/sheath boundary, as in the case of a high-recycling divertor. In this case, the loss of hot electrons to the target is compensated by the birth of cold electrons in the

ionization layer. This allows for a relatively small particle flux upstream, while maintaining a large flux through the sheath, as necessary to satisfy the Bohm criterion. A small convective flux is also consistent with our assumption that the conductive heat flux q_e is constant. The ionization layer, which is typically narrow compared to the temperature gradient length, can be treated as part of the target/sheath boundary condition. We assume that the particle flux is zero throughout the region of interest and apply Eq. (4) as a boundary condition, thereby setting the value of Γ_{e0} in Eq. (6). Assuming that f_{e0} is Maxwellian in Eq. (6), one may calculate $\Delta\Phi_{sh}$ and, in particular, one arrives at the classical result given by Eq. (5).

To see how the sheath boundary condition fixes the electron collisionality, simply combine the definition of δ with Eq. (4) to obtain

$$[q_e/(n_e T_e v_e)]_0 = \delta[(1 + T_{i0}/T_{e0})m_e/m_i]^{1/2}. \quad (10)$$

Substituting this into Eq. (3) gives the collisionality regime. Assuming deuterium ions with $T_{i0} \sim T_{e0}$ and $\delta \sim 4.8$, the result is $[q_e/(n_e T_e v_e)]_0 \sim 0.1$, which is marginally in the classical fluid regime. Furthermore, for the typical case of nearly constant pressure along the field line, the quantity $q_e/(n_e T_e v_e)$ is largest at the target/sheath boundary, decreasing like $T_e^{-1/2}$ as one progresses upstream. Hence, the lowest collisionality regime is directly in front of the target.

Specifying the density at the target/sheath boundary n_{e0} and the heat flux q_e , one may use the above equations to determine the electron temperature, i.e., Eq. (10) gives T_{e0} and (2) gives the entire profile. Consider the following example. Taking $q_e = 100 \text{ MW/m}^2$ and $n_{e0} = 2 \times 10^{20} \text{ m}^{-3}$, together with $\delta = 4.8$, gives $T_{e0} = 16 \text{ eV}$ and an upstream temperature of $T_{eu} = 74 \text{ eV}$ at $z = -30 \text{ m}$. These parameters are representative of a DIII-D high-confinement mode (H-mode)²⁰ in which case the midplane of the flux surface is about 30 m upstream of the divertor target. Figure 1 shows the relevant physical length scales at various distances from the target/sheath boundary. Here the energy-dependent MFP is defined as $\lambda_e(v/v_e)^4$ and is shown for several different values of (v/v_e) . The local gradient length L_T is also shown for comparison; as can be seen, only the most energetic electrons ($v/v_e \geq 2.7$) have a MFP which exceeds the gradient length. However, the MFP can exceed the connection length to the target, even for moderate energy electrons; for example, electrons with $v/v_e = 2$ are shown to be within a MFP of the target for the first 10 m; whereas electrons with $v/v_e = 2.25$ are within a MFP for the entire 30 m. It will be shown in Sec. V that the electron distribution function becomes non-Maxwellian in the vicinity of the target, where the MFP is comparable to the connection length.

III. KINETIC FOKKER-PLANCK APPROACH

The kinetic approach is to solve the Fokker-Planck equation for the electron distribution function $f_e(v_\perp, v_\parallel, z)$ along the magnetic field line. Here f_e is actually the gyroaveraged distribution function, v_\perp and v_\parallel are the usual cylindrical coordinates in velocity space, and z is the distance along the field line. The Fokker-Planck equation for f_e is

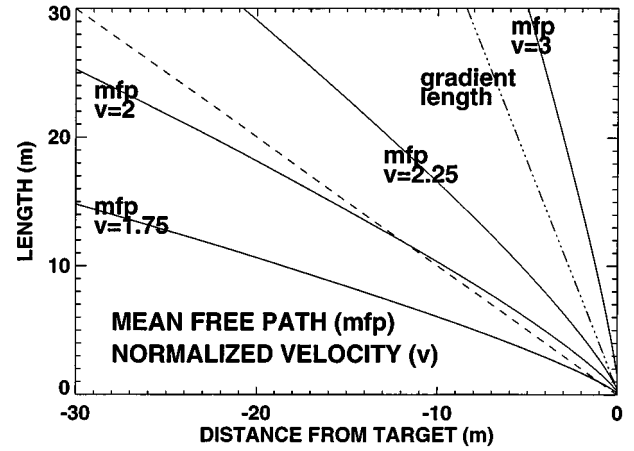


FIG. 1. Various length scales vs distance from the target/sheath boundary. The temperature profile is calculated via the fluid model in Sec. II, assuming the following two parameters $q_e = 100 \text{ MW/m}^2$ and $n_{e0} = 2 \times 10^{20} \text{ m}^{-3}$. The density profile assumes constant pressure. Here the energy-dependent mean free path (MFP) is defined as $\lambda_e(v/v_e)^4$ and is shown for various normalized velocities, $v/v_e = 1.75, 2, 2.25,$ and 3 . Electrons with $v/v_e \geq 2$ are within one MFP of the target. The local temperature gradient length L_T is also shown for comparison; only the most energetic electrons, $v/v_e \geq 2.7$, have a MFP which exceeds the gradient length.

$$\left(\frac{\partial}{\partial t} + v_\parallel \frac{\partial}{\partial z} + E_\parallel \frac{\partial}{\partial v_\parallel} \right) f_e = C(f_e) + S, \quad (11)$$

where $C(f_e)$ is the Coulomb collision operator and S represents any sources, or sinks. Here $C(f_e)$ refers to the full nonlinear collision operator (as in Ref. 21), gyro-averaged and with ions taken as a fixed Maxwellian. Since $E_\parallel(z)$ is generally unknown, an additional equation is needed. Possible methods of determining E_\parallel include solving Poisson's equation, imposing quasineutrality, or prescribing some closed form relation between E_\parallel and the moments of f_e .

Since the precise structure of the Debye sheath is not of interest here, we impose quasineutrality, together with an appropriate target/sheath boundary condition to determine $\Delta\Phi_{sh}$. Assuming that the electrical current J_\parallel is known, the relation

$$J_\parallel = \int d^3v v_\parallel e(Z_i f_i - f_e), \quad (12)$$

serves as a constraint on f_e which can be satisfied by adjusting $E_\parallel(z)$ in Eq. (11). If the ion flux and the electrical current are constant (in space and time), then Eq. (12) reduces to a constant flux condition on f_e , thereby maintaining the initial density profile throughout the time evolution of Eq. (11). For simplicity, we assume that J_\parallel is zero. More generally, the divertor target may be grounded, or biased to drive current through the SOL, and, in addition, small eddy currents may exist which allow J_\parallel to vary along the field line. As discussed in Sec. II, we assume there is a source flux of cold electrons due to ionization at the target/sheath boundary. This compensates for the loss of electrons to the target, allowing the overall particle flux to remain small. Formally constraining f_e to have zero particle flux determines the value of $E_\parallel(z)$ in Eq. (11).

Appropriate boundary conditions must be imposed at both ends of the field line. At the target/sheath boundary, electrons with $v_{\parallel} > (2e\Delta\Phi_{\text{sh}}/m_e)^{1/2}$ are absorbed by the target, otherwise they are reflected. The value of $\Delta\Phi_{\text{sh}}$ is calculated to maintain a prescribed flux of high energy electrons to the target, as set by the Bohm criterion in Eq. (4), so as to be completely consistent with the classical fluid approach outlined in Sec. II. This flux is balanced by the source of cold electrons of the target. At some specified location upstream from the target, the distribution function of incoming electrons (going toward the target) is fixed to be Maxwellian, thereby setting an effective upstream temperature. Note, the distribution of outgoing electrons at this same location upstream is not fixed, but is calculated as part of the solution. Although the upstream boundary condition appears somewhat arbitrary, it still captures the relevant physics. An alternative method would be to solve Eq. (11) with target/sheath boundary conditions applied at both ends of the field line and to specify some distributed source term to account for the influx of hot electrons from the plasma core.

IV. NUMERICAL METHOD

The kinetic equation is solved by finite difference using a two-step alternating direction implicit (ADI) relaxation scheme:

$$(f^{n+1/2} - f^n)/\Delta t + A(f^{n+1/2}) + B(E^n, f^n) = 0, \quad (13)$$

$$(f^{n+1} - f^{n+1/2})/\Delta t + A(f^{n+1/2}) + B(E^{n+1}, f^{n+1}) = 0, \quad (14)$$

where A and B are operators

$$A(f) = \left(v_{\parallel} \frac{\partial}{\partial z} \right) f,$$

$$B(E, f) = \left(E \frac{\partial}{\partial v_{\parallel}} \right) f - C(f),$$

and the subscripts on f_e and E_{\parallel} have been omitted to simplify the notation. Note that Δt is the time increment for each half-step, i.e., for $n \rightarrow n + 1/2$ and $n + 1/2 \rightarrow n + 1$. The operator A represents convection along the magnetic field line, while the operator B represents velocity space flows due to collisions and the electric field.

The z mesh extends from some upstream boundary at $z = z_u$ to the target/sheath boundary at $z = 0$. A fully centered flux-conserving difference scheme is used to represent $A(f)$. Boundary conditions at both ends of the z mesh require specification of the incoming particle fluxes. At $z = z_u$, the influx for $v_{\parallel} > 0$ is fixed to be $v_{\parallel} f_u$, where f_u is a Maxwellian

distribution of prescribed density n_{eu} and temperature T_{eu} . A standard tridiagonal system is then solved to advance Eq. (13) for $v_{\parallel} > 0$. Each point on the (θ, v) -mesh is advanced independently. At $z = 0$, the outflux for $v_{\parallel} > (2e\Delta\Phi_{\text{sh}}/m_e)^{1/2}$ is computed via Eq. (6). Note that Eq. (6) is a relation between the sheath flux Γ_{e0} and the sheath potential $\Delta\Phi_{\text{sh}}$; in our case Γ_{e0} is fixed by Eq. (4) and $\Delta\Phi_{\text{sh}}$ is calculated. To complete the target/sheath boundary condition, the incoming particle flux for negative v_{\parallel} must be specified. Since electrons with $0 < v_{\parallel} < (2e\Delta\Phi_{\text{sh}}/m_e)^{1/2}$ are reflected, part of the influx is automatically specified. The remaining influx is specified as $v_{\parallel} f_c$ (for $v_{\parallel} < 0$) where f_c is a cold Maxwellian representing the ionization source. The temperature of f_c is chosen to be cold in comparison to the sheath temperature. The normalization of f_c is determined by requiring

$$\int_{v_{\parallel} < 0} v_{\parallel} f_c d^3v = -\Gamma_{e0},$$

thereby imposing zero net flux at the boundary. A standard tridiagonal system is then solved to advance Eq. (13) for $v_{\parallel} < 0$.

A nine-point flux-conserving difference scheme is used to represent $B(E, f)$.²² The finite-difference scheme actually employs (θ, v) coordinates in velocity space, with $v_{\perp} = v \sin \theta$ and $v_{\parallel} = v \cos \theta$. The v mesh is truncated at some maximum energy, large compared to the upstream temperature, where an outflux boundary condition is applied, i.e., phase space density flows freely off the edge of the grid. The total number of particles lost at the v -mesh boundary is typically negligible, verifying that mesh truncation does not effect the integrity of the solution.

The term $B(E^{n+1}, f^{n+1})$ in Eq. (14) includes two types of nonlinearities. The collision operator is nonlinear, since the Fokker-Planck coefficients for electron-electron collisions depend on integrals over the unknown distribution function. Within the context of our ADI relaxation scheme, this is handled by making the replacement $f^{n+1} \rightarrow f^{n+1/2}$ in all such collision integrals. A second nonlinearity enters through the electric field term, involving the product of two unknowns E^{n+1} and f^{n+1} , where the additional equation for E^{n+1} takes the form of an integral constraint on f^{n+1} , namely

$$\int v_{\parallel} f^{n+1} d^3v = 0.$$

TABLE I. Comparison of results from three FPET runs: T_{eu} is the temperature (in eV) of the incoming Maxwellian at the upstream boundary, T_{e0} is the temperature at the target/sheath boundary, and $(T_{e0})_f$ is the corresponding sheath temperature calculated from classical fluid theory, as discussed in the text. The sheath potential $\Delta\Phi_{\text{sh}}$ is given in eV. The following normalized parameters are also shown: $\phi = e\Delta\Phi_{\text{sh}}/T_{e0}$, $\delta = q_{e0}/(\Gamma_{e0}T_{e0})$, $\bar{q}_0 = q_{e0}/(n_{e0}v_{e0}T_{e0})$, $\bar{q}_u = q_{eu}/(n_{eu}v_{eu}T_{eu})$, and λ_{eu}/L , where λ_{eu} is the thermal MFP evaluated at the upstream boundary, and L is the connection length to the target. For comparison, the classical values of ϕ and δ are approximately 2.8 and 4.8, respectively, in all three cases.

Run	T_{eu}	T_{e0}	$(T_{e0})_f$	$\Delta\Phi_{\text{sh}}$	ϕ	δ	\bar{q}_0	\bar{q}_u	λ_{eu}/L
1	74	11	14	35	3.2	6.1	0.17	0.038	0.052
2	108	18	30	61	3.4	8.2	0.22	0.069	0.107
3	140	28	53	104	3.7	9.4	0.24	0.098	0.178

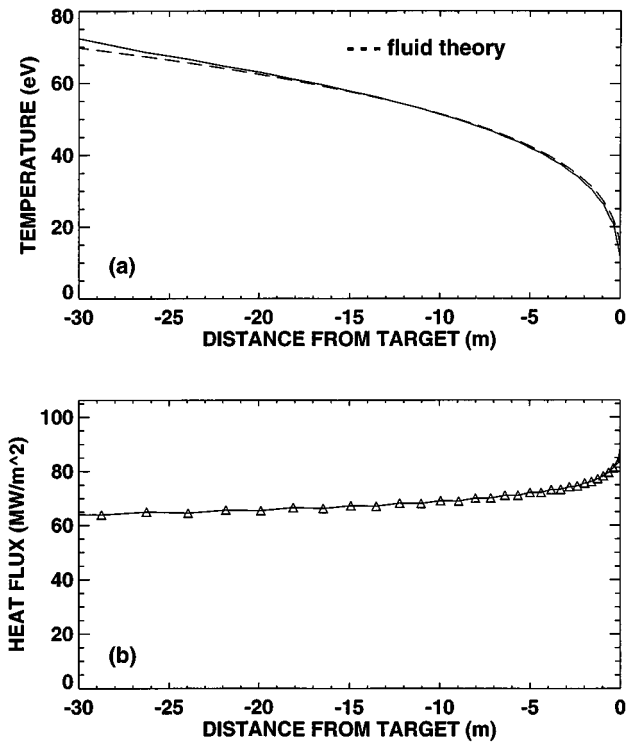


FIG. 2. Results of FPET run 1 showing (a) the temperature profile and (b) the parallel heat flux (MW/m^2). In (a) the kinetic solution from FPET is compared to conventional fluid theory (dashed line) for the same heat flux. At the upstream boundary, the kinetic T_e profile diverges somewhat from the fluid profile; this is an artifact of the numerical boundary condition, which imposes a Maxwellian distribution for incoming electrons. The triangles in (b) show mesh points of the numerical simulation. Note, that the heat flux incident to the surface of the target is $q_{e\parallel} \sin \alpha$, where α is the small grazing angle of the field line with respect to the target.

(Note, the constraint must be applied at each z -mesh point along the magnetic field line.) The solution is obtained by linearizing Eq. (14) as follows:

$$\begin{aligned} & \frac{(f^{n+1} - f^{n+1/2})}{\Delta t} + B(E^n, f^{n+1}) \\ &= -A(f^{n+1/2}) - \Delta E \left(\frac{\partial}{\partial v_{\parallel}} \right) f^{n+1/2}, \end{aligned}$$

where $\Delta E \equiv E^{n+1} - E^n$. Upon setting $f^{n+1} = h + g \Delta E$, one obtains independent equations for h and g

$$h/\Delta t + B(E^n, h) = f^{n+1/2}/\Delta t - A(f^{n+1/2}),$$

$$\frac{g}{\Delta t} + B(E^n, g) = - \left(\frac{\partial}{\partial v_{\parallel}} \right) f^{n+1/2}.$$

Notice that these equations involve the same operator on the left-hand side. Within the context of our finite difference scheme, this operator is represented as a banded matrix and factored once to compute both h and g . The SLATEC (LINPACK)²³ routines SBGCO and SGBS were used to factor the band matrix by Gaussian elimination and solve the linear system of equations. The updated electric field is then determined as

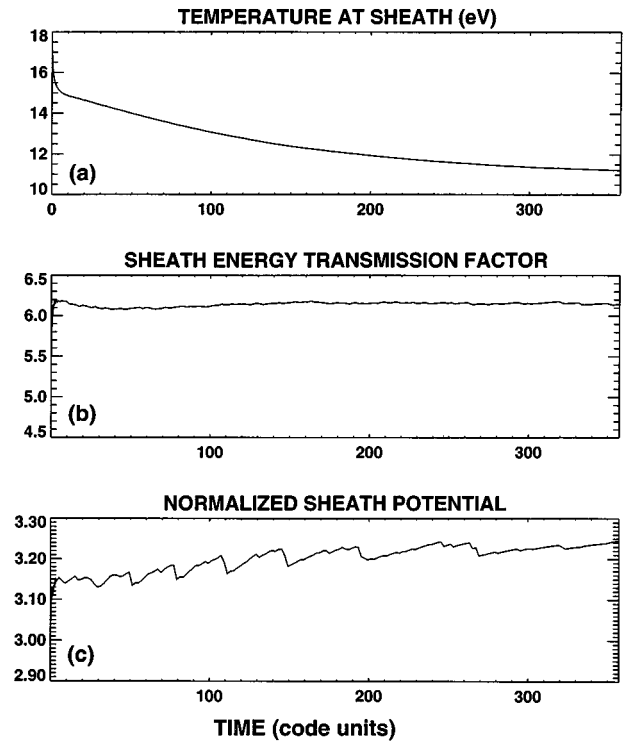


FIG. 3. Time evolution of FPET run 1 showing (a) temperature at sheath T_{e0} , (b) energy transmission factor δ , and (c) normalized sheath potential ϕ , as functions of time. The time is specified in code units, defined as the length of the field line (30 m) divided by the maximum velocity mesh point [approximately $4(T_{eu}/m_e)^{1/2}$].

$$E^{n+1} = E^n - \left(\int d^3v v_{\parallel} h \right) \left(\int d^3v v_{\parallel} g \right)^{-1}.$$

There are two alternatives for updating the distribution function; we can either accept the solution of the linearized equation, i.e., $h + g \Delta E$, or we can recompute the solution of Eq. (14) using the above value for E^{n+1} . Since the later algorithm is stable for arbitrary Δt , it generally justifies the additional computation required on each time step.

It is important to point out that each grid point on the z mesh is advanced independently in Eq. (14), allowing large gains in overall speed to be obtained through parallel processing. The two-dimensional velocity space step Eq. (14) takes much more computation than the one-dimensional configuration space step Eq. (13). In a CRAY T3D parallel processing implementation of the code, we solve Eq. (14) on separate processors for each space point. The space equation, Eq. (13), is solved across processors. For 30 space points (and 64 v points, 32 θ points) the code is executed in 750 s using 8 processors, and 240 s using 32 processors. Thus, as the number of processors was increased by a factor of 4, there was a factor of 3.1 overall speedup. Limits on speedup are yet to be explored.

V. COMPARISON OF KINETIC AND FLUID SOLUTIONS

To compare kinetic solutions with classical fluid solutions, we chose a set of three FPET runs: each run documents

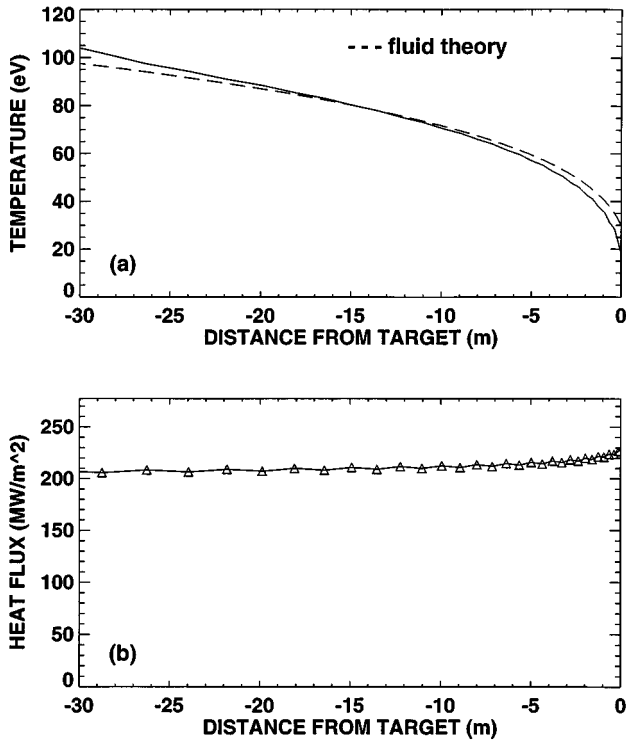


FIG. 4. Results of FPET run 2 showing (a) the temperature profile and (b) the parallel heat flux (MW/m^2). In (a) the kinetic solution from FPET is compared to conventional fluid theory (dashed line) for the same heat flux. The triangles in (b) show mesh points of the numerical simulation.

an increasing departure from classical fluid theory. In all three runs, the density profile was taken to be

$$n_e = n_{e0}(1 - \alpha z)^{-2/7}, \quad (15)$$

with $n_{e0} = 2 \times 10^{20} \text{ m}^{-3}$ and $\alpha = 9.284 \text{ m}^{-1}$, to give an upstream density of $n_{eu} = 4 \times 10^{19} \text{ m}^{-3}$ at $z_u = -30 \text{ m}$. The electric field was calculated to give zero particle flux, thereby maintaining the density profile. The temperature of the cold Maxwellian particle source at the target/sheath boundary was taken to be 3 eV in all three runs. Upstream, the incoming distribution function was taken to be a Maxwellian with density n_{eu} and temperature T_{eu} . The upstream temperature was increased in each of the three runs, steady-state solutions were obtained, and parameters such as the target/sheath temperature and energy transmission factor were calculated. The results are summarized in Table I. Detailed comparisons to fluid theory are discussed below.

Results of the first run are shown in Figs. 2 and 3. Here the parameters are very close to the DIII-D example discussed at the end of Sec. II, so the length scales in Fig. 1 still apply. Figure 2(a) shows the T_e profile, where T_e is calculated from the distribution function,

$$T_e = \frac{m_e}{3n_e} \int d^3v v^2 f_e.$$

The heat flux, shown in Fig. 2(b), is nearly constant along the field line, as would be expected in steady state. It is noteworthy, however, that the heat flux is not precisely constant. The steady increase seen in Fig. 2(b) is actually due to

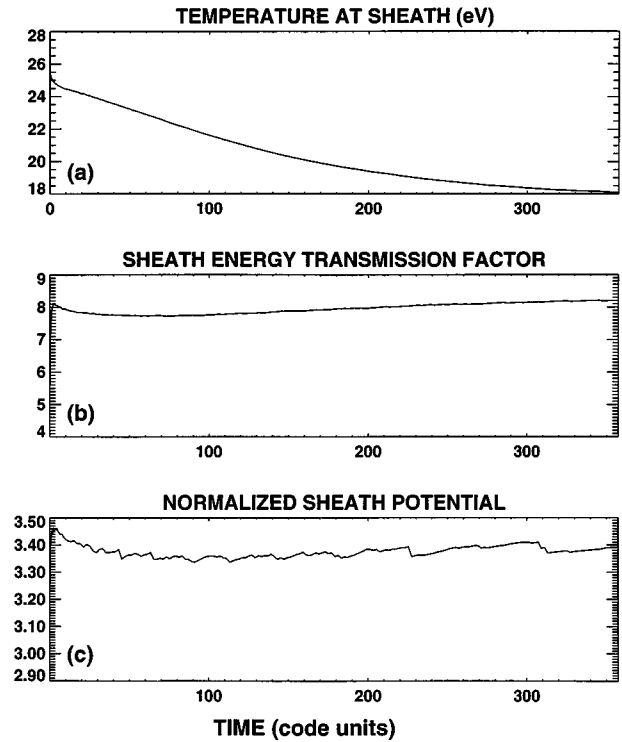


FIG. 5. Time evolution of FPET run 2 showing (a) temperature at sheath T_{e0} , (b) energy transmission factor δ , and (c) normalized sheath potential ϕ , as functions of time. The time is specified in code units, defined as the length of the field line (30 m) divided by the maximum velocity mesh point [approximately $4(T_{eu}/m_e)^{1/2}$].

discretization errors involving the collision operator, as will be discussed in more detail below. Figure 3 shows the time evolution of the temperature (and other parameters) at the sheath edge. The system relaxes quickly at first and then gradually approaches a true steady state. [Fluctuations of the normalized sheath potential visible in Fig. 3(c) are artifacts of the relaxation scheme. These fluctuations are so small, note the scale of Fig. 3(c), as to be insignificant.] Also shown in Fig. 2(a) is the fluid temperature profile calculated for the same parameters. This is done by integrating Eq. (1) numerically using the q_e profile determined by FPET, i.e., as shown in Fig. 2(b). (The variation of the Coulomb logarithm is also properly treated in the numerical integration.) Integration proceeds from the target/sheath boundary and continues upstream. The appropriate fluid value for T_{e0} is calculated from Eq. (10), where δ is taken to be approximately 4.8, as discussed in Sec. II. The fluid values for T_{e0} are also shown in Table I. Although the kinetic and fluid T_e profiles are in close agreement for run 1, the kinetic effects are exaggerated in runs 2 and 3, leading to considerable differences between the two profiles in the vicinity of the target. The results for run 2 are shown in Figs. 4 and 5. The results for run 3 are shown in Figs. 6 and 7.

The velocity space mesh for all three runs consisted of 200 v points and 50 θ points. A dense grid in v is necessary to accurately represent both the bulk and tail of the distribution function, especially in the case of a large temperature gradient. One type of discretization error in this system involves the nonlinear collision operator, which spuriously

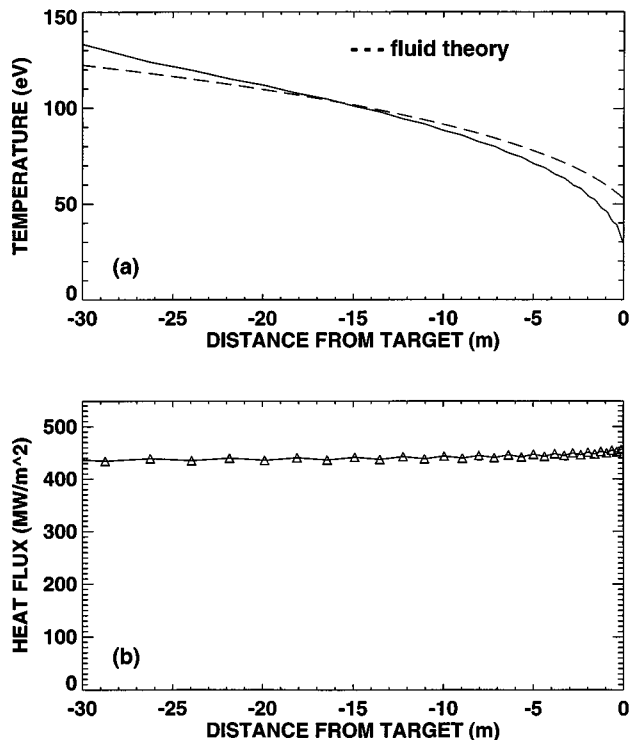


FIG. 6. Results of FPET run 3 showing (a) the temperature profile and (b) the parallel heat flux (MW/m^2). In (a) the kinetic solution from FPET is compared to conventional fluid theory (dashed line) for the same heat flux. The triangles in (b) show mesh points of the numerical simulation.

generates a certain amount of energy. The effect manifests itself in Fig. 2(b) as a small, but steady increase in the heat flux. The magnitude of this numerically generated energy source depends on the velocity space mesh, which is the same for each of the three runs. Therefore, in a situation where the temperature gradient is large, corresponding to a large physical heat flux, the spurious contribution is relatively small, as in Fig. 6(b).

Several interesting facts can be discerned from Table I and Figs. 2–7. In Sec. II we argued that the divertor has a single collisionality regime, i.e., that λ_e/L_T should be independent of the heat flux, or density. This argument was based on fluid theory combined with classical target/sheath boundary conditions. In fact, however, kinetic solutions show an increasing departure from fluid theory as the heat flux is increased. This is because the upstream temperature is increased, thereby increasing the MFP, while the connection length to the target remains fixed. As a result, the distribution function in the target/sheath region becomes rich in superthermal electrons and increasingly nonisotropic (see Figs. 8 and 9). The distortion of the distribution function also modifies the way the heat flux is distributed in energy, i.e., near the target the heat flux is carried by a larger relative fraction of energetic electrons, as shown in Fig. 10. Since δ is a measure of the energy carried by electrons escaping through the sheath [see Eqs. (7) and (8)], its value is dramatically enhanced by these non-Maxwellian features. It is easy to see that an increase in δ must lead to a corresponding drop in T_{e0} , when compared to the fluid value, because both q_{e0} and

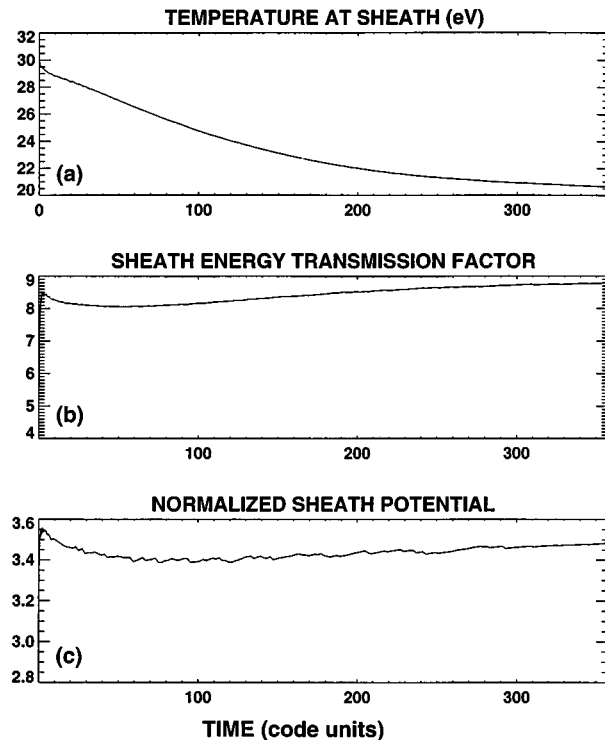


FIG. 7. Time evolution of FPET run 3 showing (a) temperature at sheath T_{e0} , (b) energy transmission factor δ , and (c) normalized sheath potential ϕ , as functions of time. The time is specified in code units, defined as the length of the field line (30 m) divided by the maximum velocity mesh point [approximately $4(T_{eu}/m_e)^{1/2}$].

Γ_{e0} are fixed in the comparison. Furthermore, since T_{e0} is reduced, but ϕ remains approximately constant, the physical value of $\Delta\Phi_{\text{sh}}$ is also reduced in comparison to the classical value. For example, in run 3 the classical value of $\Delta\Phi_{\text{sh}}$ is 162 eV, whereas the kinetic value is 105 eV, a considerable difference.

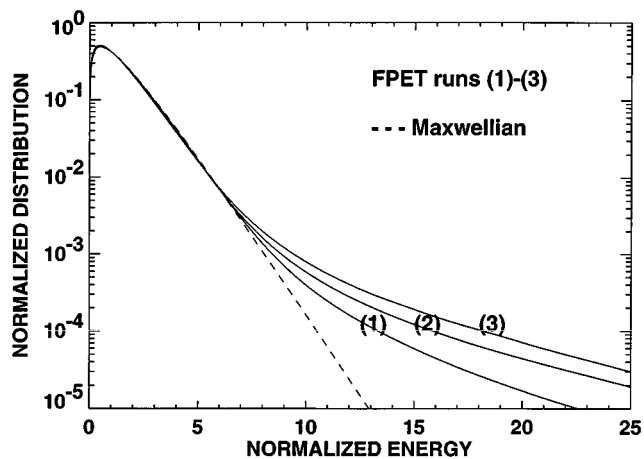


FIG. 8. Normalized distribution function near the target/sheath boundary vs normalized energy for each of the three FPET runs. The normalized energy is $E = m_e v^2 / (2T_e)$, where T_e is evaluated locally. The distribution functions are integrated over pitch angle and rescaled to give unity when integrated over E . A Maxwellian distribution is shown for comparison. A superthermal tail is visible in each of the three runs, becoming more dramatic as the heat flux increases.

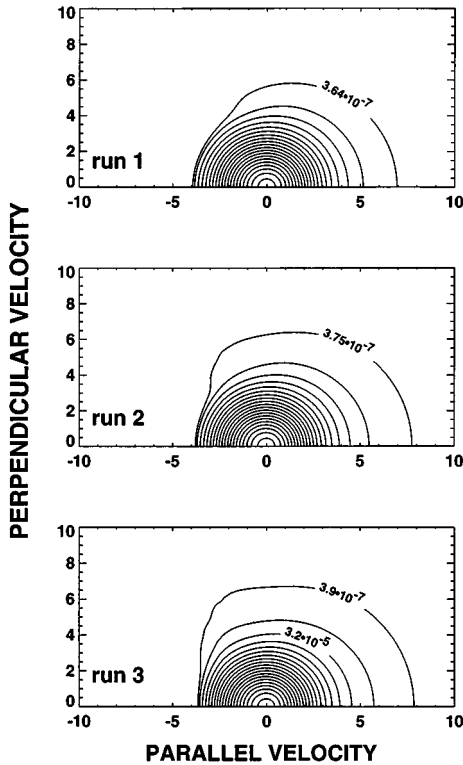


FIG. 9. Contour plots of the normalized distribution function near the target/sheath boundary for each of the three FPET runs. The velocities are normalized to the local thermal velocity $v_e = (T_e/m_e)^{1/2}$. The distribution functions are rescaled by the factor $v_e^3 n_e^{-1}$. Because energetic electrons are absorbed by the target, the distribution functions are depleted of energetic electrons propagating upstream, i.e., with negative v_{\parallel} . Lower energy electrons traveling toward the target are reflected by the sheath potential and fill in the depleted region through pitch-angle scattering. Note, the spatial position shown here is 12 cm upstream of the target.

In the above discussion we emphasized the role of kinetic effects on the target/sheath boundary boundary condition. These effects seem to be independent of any kinetic modifications to the thermal conductivity. To demonstrate this, we recalculated the fluid T_e profile using the kinetic value of T_{e0} as a boundary condition (BC) in Eq. (1). [Using the kinetic value of T_{e0} is equivalent to assuming the kinetic value of δ and recalculating T_{e0} from Eq. (10).] With the adjusted BC the fluid T_e profile accurately tracks the kinetic profile for 10–15 m upstream of the target, as shown in Fig. 11. We therefore conclude, in the case of a simple divertor, that classical thermal conductivity is nearly correct and that only modest flux-limiting,^{2,9} or nonlocal corrections^{3–8} would be required to accurately model the kinetic T_e profile farther upstream. For the model studied in this paper, the major correction to fluid theory arises in the sheath boundary condition. In more general divertor studies, however, strong radiation cooling of electrons may lead to steeper temperature profiles, requiring more significant modifications of the thermal conductivity.

VI. CONCLUSIONS

Electron transport along open field lines in the diverted scrape-off layer of a tokamak has been studied numerically with the Fokker–Planck edge transport code (FPET). The

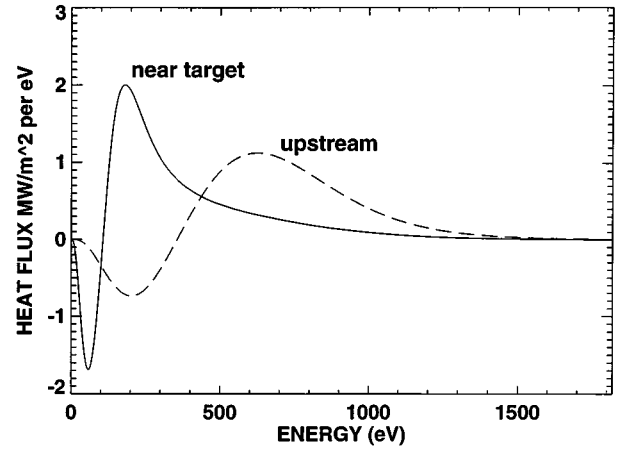


FIG. 10. Heat flux (MW/m^2 per eV) vs energy (eV) at two points along the field line—near the target/sheath boundary and near the upstream boundary—for FPET run 3. The normalized energy of the positive peak is 4.75 at the upstream location and 5.73 near the target. Recall that the normalized energy is $m_e v^2 / (2T_e)$, where T_e is evaluated locally, as in Fig. 8. The distribution of heat flux near the target is shifted toward higher normalized energy and contains a high energy tail due to free-streaming electrons from upstream.

code gives a proper kinetic treatment of the competition between free streaming along the field line and collisional scattering in velocity space. The electrostatic field is calculated by imposing quasineutrality along the entire field line. The potential drop across the target/sheath boundary is calculated by restricting the electron flux escaping through the sheath. The sheath itself, however, is not resolved. Rather, the Debye sheath, the ion gyrosheath, and the ionization layer in front of the target are all compressed into one boundary condition that requires specifying the electron flux to the target.

Kinetic results obtained with FPET have been compared to classical fluid results for the case of a simple (nonradia-

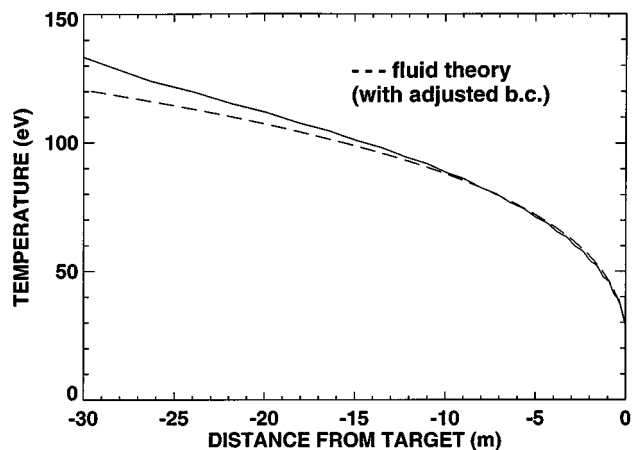


FIG. 11. Temperature profile from FPET run 3, as in Fig. 6(a), but now compared to fluid theory with an adjusted boundary condition that assumes the kinetic value of T_{e0} . With the adjusted BC the fluid T_e profile accurately tracks the kinetic profile for 10–15 m upstream of the target. Note that the difference between the two profiles is exaggerated near the upstream boundary. This is because the kinetic simulation imposes a Maxwellian distribution for incoming electrons, an unnatural boundary condition since the distribution function is actually carrying a substantial heat flux.

tive) divertor. We find that the free streaming of electrons from the midplane of the SOL creates a surplus of superthermal electrons in the vicinity of the target. As a result, the sheath energy transmission factor is enhanced relative to the classical (Maxwellian) value and the bulk electron temperature is lowered relative to the classical value. In comparing kinetic and fluid results, we find that classical thermal conductivity is approximately correct in describing the steady-state T_e profile of a simple divertor, provided that the sheath temperature is taken from the kinetic simulation. Therefore, in our simulations, the main importance of the non-Maxwellian character of the distribution function is to modify the target/sheath boundary physics. Since superthermal electrons escaping through the sheath contribute so strongly to the overall heat flux, it is inevitable that the bulk electron temperature falls in response, otherwise a constant heat flux cannot be maintained. Furthermore, this result does not depend on the detailed structure of the boundary layer, i.e., the Debye sheath, the ion gyrosheath, and the ionization layer, rather it is a straightforward consequence of energy balance and particle balance: energetic electrons that escape through the sheath are replaced by cool electrons born in the ionization layer. A lower bulk electron temperature in the vicinity of the target results in a smaller potential drop across the sheath, since the two are roughly proportional. The precise relation between the sheath potential and the electron temperature, however, depends on detailed modeling of the boundary layer. This is important because the sheath potential largely determines the energy with which ions impact the target, thereby affecting the rate of target erosion.

In conclusion, we report the development of a new kinetic transport code for parallel transport in the scrape-off layer. Using this code to study a simple nonradiative divertor configuration we discovered that the electron distribution function in the vicinity of the target is modified in two ways: (i) there is a non-Maxwellian tail, or surplus of superthermal particles, and (ii) the bulk temperature is reduced. These results will have to be included in more detailed divertor studies to uncover their full implication, but we anticipate a strong effect on ionization rates and radiation rates from impurities in the vicinity of the target, as determined by the

energy dependence of each individual cross section relative to the electron temperature and the population of superthermals.

ACKNOWLEDGMENTS

This is a report of research and work supported by the U.S. Department of Energy under Grant No. DE-FG03-95ER54309 and Contract No. DE-AC03-89ER51114, and in part by an appointment to the U.S. Department of Energy Fusion Energy Postdoctoral Research Program at General Atomics administered by the Oak Ridge Institute for Science and Education. The work was also supported in part by the Swiss National Science Foundation.

- ¹L. Spitzer, Jr. and R. Harm, *Phys. Rev.* **89**, 977 (1953).
- ²S. A. Khan and T. D. Rognlien, *Phys. Fluids* **24**, 1442 (1981).
- ³J. F. Luciani, P. Mora, and J. Virmont, *Phys. Rev. Lett.* **51**, 1664 (1983).
- ⁴P. M. Campbell, *Phys. Rev. A* **30**, 365 (1984).
- ⁵J. F. Luciani, P. Mora, and R. Pellat, *Phys. Fluids* **28**, 835 (1985).
- ⁶J. R. Albritton, E. A. Williams, I. B. Bernstein, and K. P. Swartz, *Phys. Rev. Lett.* **57**, 1887 (1986).
- ⁷E. M. Epperlein, *Phys. Rev. Lett.* **65**, 2145 (1990).
- ⁸S. I. Krashennnikov, *Phys. Fluids B* **5**, 74 (1993).
- ⁹T. D. Rognlien, *Bull. Am. Phys. Soc.* **34**, 1981 (1989).
- ¹⁰R. Chodura, *Contrib. Plasma Phys.* **32**, 219 (1992).
- ¹¹R. J. Procassini and C. K. Birdsall, *Phys. Fluids B* **3**, 1876 (1991).
- ¹²R. J. Procassini, C. K. Birdsall, and B. I. Cohen, *Nucl. Fusion* **30**, 2329 (1990).
- ¹³O. Sauter, R. W. Harvey, and F. L. Hinton, *Contrib. Plasma Phys.* **34**, 169 (1994).
- ¹⁴S. I. Braginskii, in *Review of Plasma Physics*, edited by M. A. Leontovich (Consultants Bureau, New York, 1965), Vol. I, p. 205.
- ¹⁵P. C. Stangeby and G. M. McCracken, *Nucl. Fusion* **30**, 1225 (1990).
- ¹⁶P. C. Stangeby, *Phys. Plasmas* **2**, 702 (1995).
- ¹⁷P. C. Stangeby, *Phys. Plasmas* **2**, 707 (1995).
- ¹⁸R. H. Cohen and D. D. Ryutov, *Phys. Plasmas* **2**, 2011 (1995).
- ¹⁹R. H. Cohen and D. D. Ryutov, *Plasma Phys. Controlled Fusion* **16**, 225 (1995).
- ²⁰J. Watkins, *J. Nucl. Mater.* **220-222**, 347 (1995).
- ²¹F. L. Hinton, in *Handbook of Plasma Physics*, edited by M. N. Rosenbluth and R. Z. Sagdeev (North-Holland, New York, 1983), Vol. 1, p. 147.
- ²²R. W. Harvey and M. G. McCoy, in *Proceedings of the IAEA Technical Committee Meeting on Simulation and Modeling of Thermonuclear Plasma, Montreal, 1992* (International Atomic Energy Agency, Vienna, 1993), p. 489; G. D. Kerbel and M. B. McCoy, *Phys. Fluids* **28**, 3629 (1985).
- ²³W. H. Vandevender and K. H. Haskell, *SIGNUM Newslett.* **17**(3), 16 (1993).